Memory and synaptic deficits in *Hip14/DHHC17* knockout mice

Austen J. Milnerwood[a,b,1,2], Matthew P. Parsons[a,b,1], Fiona B. Young[c], Roshni R. Singaraja[c], Sonia Franciosi[c], Mattia Volta[d], Sabrina Bergeron[d], Michael R. Hayden[c], and Lynn A. Raymond[a,b,3]

[a]Department of Psychiatry and [b]Brain Research Centre, University of British Columbia, Vancouver, BC, Canada V6T 1Z3; [c]Centre for Molecular Medicine and Therapeutics, University of British Columbia, Vancouver, Canada V5Z 4H4; and [d]Centre for Applied Neurogenetics and Translational Neuroscience, Division of Neurology, Department of Medicine, University of British Columbia, Vancouver, BC, Canada V6T 2B5

Edited by Richard L. Huganir, The Johns Hopkins University School of Medicine, Baltimore, MD, and approved October 29, 2013 (received for review January 3, 2013)

Palmitoylation of neurotransmitter receptors and associated scaffold proteins regulates their membrane association in a rapid, reversible, and activity-dependent fashion. This makes palmitoylation an attractive candidate as a key regulator of the fast, reversible, and activity-dependent insertion of synaptic proteins required during the induction and expression of long-term plasticity. Here we describe that the constitutive loss of huntingtin interacting protein 14 (Hip14, also known as DHHC17), a single member of the broad palmitoyl acyltransferase (PAT) family, produces marked alterations in synaptic function in varied brain regions and significantly impairs hippocampal memory and synaptic plasticity. The data presented suggest that, even though the substrate pool is overlapping for the 23 known PAT family members, the function of a single PAT has marked effects upon physiology and cognition. Moreover, an improved understanding of the role of PATs in synaptic modification and maintenance highlights a potential strategy for intervention against early cognitive impairments in neurodegenerative disease.

striatum | hippocampus | posttranslational modification | long-term potentiation | Huntington disease

Palmitoylation is a posttranslational protein modification increasingly recognized as an important regulator of neuronal development, synaptic function, and plasticity (1, 2). Palmitoyl acyltransferase (PAT) enzymes regulate membrane association of proteins by catalyzing the addition of the fatty acid palmitate to cysteines via thioester bonds. Palmitoylation is readily reversible, making it an attractive candidate for a regulator of the rapid synaptic protein trafficking required for synaptic transmission and plasticity. The growing list of palmitoylated neuronal substrates includes scaffolds, ion channels, and vesicle-associated proteins, and their palmitoylation status can have dramatic effects on function and/or localization within membranes. For example, synaptic activity dynamically regulates palmitoylation of postsynaptic density protein-95 (PSD-95), influencing its clustering at postsynaptic sites (3–5), whereas palmitoylation of NMDA-and AMPA-type glutamate receptor subunits regulates their insertion, removal, and stabilization in the postsynaptic membrane (6–9). The importance of this modification within the brain is highlighted by implication of palmitoylation deficits in a number of neurological diseases including Alzheimer's disease, schizophrenia, and Huntington disease (HD) (10).

To date, 23 DHHC proteins have been identified in humans. The PAT HIP14 (DHHC17) is enriched in the brain and has a number of known synaptic substrates including PSD-95, GluA1/2, GAD-65, SNAP-25, and synaptotagmin I (11–13), suggesting roles in pre- and postsynaptic function. Indeed, Hip14 siRNA reduces PSD-95 clustering in hippocampal cultures (12), and Hip14 loss-of-function impairs neurotransmitter release in *Drosophila* (14). Interestingly, Hip14 function is impaired in HD (15, 16), suggesting that some synaptic deficits observed in this disease (17–23) may arise from hypopalmitoylation of Hip14 substrates. In support of this, we recently reported the generation of *Hip14* knockout mice, which share some interesting similarities to late-stage HD mouse models in behavioral, biochemical, and neuropathological measures (11). However, it remains unknown whether the loss of this single PAT can result in synaptic and plastic deficits reminiscent of disease states.

Here we investigate the consequences of a single PAT knockout on neuronal physiology, synaptic signaling, and plasticity. We report that *Hip14* knockout results in marked cellular and synaptic alterations in striatal spiny projection neurons (SPNs) and impaired hippocampal long-term potentiation (LTP). Furthermore, performance in a hippocampal-dependent learning paradigm was also significantly impaired. In conclusion, the constitutive absence of Hip14/DHHC17 results in major neurophysiological deficits and associated cognitive dysfunction.

Results

Altered SPN Membrane Properties and Excitability. Hip14 dysfunction has been implicated in the pathogenesis of HD (11). As striatal physiology is well characterized in various HD models (17, 18), we first used whole-cell patch clamp recordings to examine the consequences of *Hip14* knockout on cellular and synaptic properties of SPNs, the most vulnerable cell type in HD. Due to the ~20% loss of striatal cells in these mice (11), in addition to targeting SPNs based on their characteristic somatic diameter (8–16 μm) and ellipsoid morphology (Fig. 1*A*) (24), selection criteria were validated by current-clamp recordings in K^+-based internal solution. Of 17 cells recorded under these conditions (animals aged postnatal day: WT, 25 ± 1; *Hip14*$^{-/-}$,

Significance

Palmitoylation can influence the subcellular localization of various synaptic proteins; this process is therefore increasingly recognized as an important regulator of basal synaptic communication as well as activity-dependent synaptic plasticity. Despite the fact that in vitro experiments indicate that many synaptic proteins can be palmitoylated by more than one palmitoyl acyltransferase (PAT), the enzymes responsible for palmitoylation, we describe in this paper various synaptic, plastic, and cognitive consequences that result from constitutive loss of a single PAT, namely Hip14/DHHC17. This reveals an important functional role for this PAT that cannot be compensated for by other existing PATs.

Author contributions: A.J.M., M.P.P., F.B.Y., R.R.S., M.R.H., and L.A.R. designed research; A.J.M., M.P.P., F.B.Y., S.F., M.V., and S.B. performed research; A.J.M., M.P.P., F.B.Y., and S.F. analyzed data; and A.J.M. and M.P.P. wrote the paper.

The authors declare no conflict of interest.

This article is a PNAS Direct Submission.

[1]A.J.M. and M.P.P. contributed equally to this article.

[2]Present address: Centre for Applied Neurogenetics and Translational Neuroscience, Division of Neurology, Department of Medicine, University of British Columbia, Vancouver, BC, Canada V6T 2B5.

[3]To whom correspondence should be addressed. E-mail: lynn.raymond@ubc.ca.

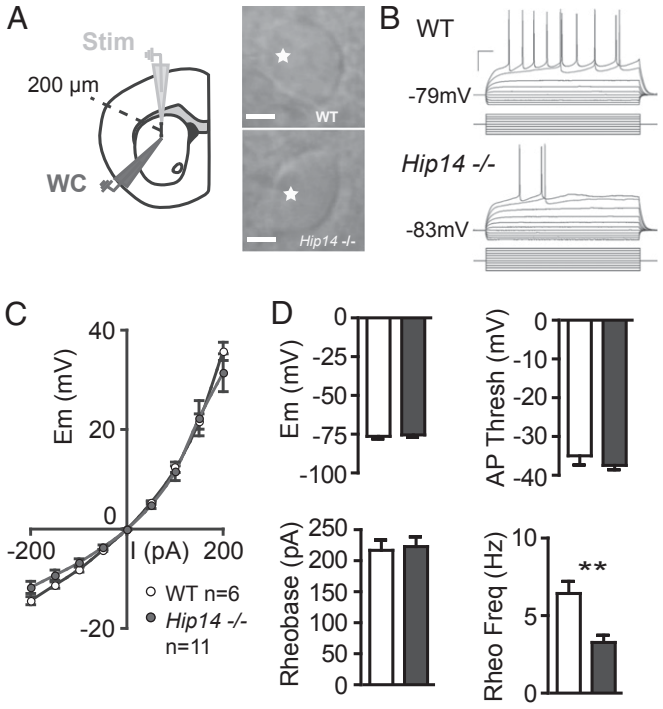

Fig. 1. Recording of SPNs in acute coronal sections and reduced action potential firing. (*A*) Striatal recording configuration (*Left*); SPNs in the central dorsal striatum were targeted for whole-cell patch clamp in acute coronal slices (*Right*). (Scale bar, 5 um.) An asterisk indicates a microelectrode tip. (*B*) Example of current-clamp membrane potential responses (*Upper*) to 50-pA current injection steps (*Lower* and in *C*) in WT and *Hip14*$^{-/-}$ SPNs; *Hip14*$^{-/-}$ SPNs fired fewer action potentials (APs) at rheobase (gray traces) despite similar I–V relationships (*B* and *C*). (Scale bar in *B*: 30 mV/400 pA, 100 ms.) (*D*) There were no differences in Em, AP threshold (thresh), or rheobase current. However, *Hip14*$^{-/-}$ mice responded with significantly fewer action potentials at rheobase (rheo freq). **t* test.

27 ± 1), all exhibited membrane properties consistent with striatal SPNs and characteristic I–V relationships exhibiting pronounced inward rectification (Fig. 1*B*) (25). Current-voltage relationships were not significantly different between genotypes (Fig. 1 *B* and *C*) nor were resting membrane potential (Em, $P = 0.51$), action potential threshold ($P = 0.42$), or rheobase ($P = 0.91$); however, SPNs from *Hip14*$^{-/-}$ mice were less excitable, with fewer action potentials at rheobase ($P = 0.009$; Fig. 1 *B* and *D*).

Voltage-clamp recordings (caesium-based solution) were then conducted to measure membrane properties and currents. Membrane capacitance (C_m) and decay time constants (τ_m) were significantly reduced in SPNs from *Hip14*$^{-/-}$ mice (C_m: WT, 106.6 ± 2.4 pF, $n = 21$ vs. *Hip14*$^{-/-}$, 94.3 ± 4.5 pF, $n = 18$, $P = 0.005$; τ_m: WT, 2.5 ± 0.1 ms, $n = 18$ vs. *Hip14*$^{-/-}$, 2.1 ± 0.1, $n = 24$, $P = 0.03$), whereas input resistance (R_m) was significantly increased (WT, 116.8 ± 6.7 MΩ, $n = 21$ vs. *Hip14*$^{-/-}$, 177.1 ± 16.1 MΩ, $n = 24$, $P = 0.005$). R_m, τ_m, and C_m are determined by plasma membrane area, and C_m is commonly interpreted as an indirect measure of cell surface area (26). Together, these data suggest that SPNs from *Hip14*$^{-/-}$ mice are less excitable than those of WT littermates and have a reduced surface membrane area.

Reduced Spontaneous and Evoked Excitatory Transmission to SPNs. To assay excitatory synaptic function, we recorded AMPA receptor (AMPAR)-mediated spontaneous excitatory postsynaptic currents (sEPSCs; $V_{hold} = -70$ mV) from SPNs in the presence of the $GABA_A$ antagonist picrotoxin (100 μM; Fig. 2*A*). Although we found no difference in mean sEPSC amplitude ($P = 0.13$), cumulative probabilities revealed a significant genotype–amplitude interaction ($P = 0.008$, two-way repeated measures ANOVA (RM-ANOVA; Fig. 2*B*), due to an increased percentage of large events in *Hip14*$^{-/-}$ SPNs (>30 pA, $P = 0.02$; Fig. 2*B*). There was a significant reduction in mean sEPSC frequency ($P = 0.03$) and longer interevent intervals (IEIs) in SPNs of *Hip14*$^{-/-}$ mice (genotype $P = 0.04$; Fig. 2*C*), consistent with the decreased excitatory synapse number that we observed previously in the striatum by electron microscopy (11).

To further investigate transmission at SPN excitatory synapses, a stimulating electrode (200–250 μm dorsal to the recording) was used to evoke EPSCs [evoked EPSCs (eEPSCs)]. In SPNs held at -70 mV, eEPSCs were evoked at increasing stimulus intensities (20, 50, and 150 μA; Fig. 2 *D* and *E*). AMPAR-mediated eEPSC peak amplitudes were reduced (genotype $P = 0.009$, two-way RM-ANOVA, Bonferroni post hoc 150 μA; Fig. 2*E*) whereas paired-pulse facilitation (PPF) was increased (genotype $P = 0.005$, two-way RM-ANOVA; Fig. 2*G*) in SPNs from *Hip14*$^{-/-}$ mice. As sEPSC amplitude was not reduced in *Hip14*$^{-/-}$ SPNs, smaller evoked currents are likely a reflection of both (*i*) reduced synapse number and (*ii*) a lower probability of release (Pr) at remaining synapses indicated by increased PPF. Thus, in the absence of Hip14, SPNs receive fewer excitatory contacts, and remaining excitatory synapses have a reduced Pr.

To determine whether Hip14 is essential for normal NMDA receptor (NMDAR) function in SPNs, dual AMPAR/NMDAR eEPSCs were evoked while cells were depolarized (V_h + 60 mV; Fig. 2*D*) and NMDAR current (I_{NMDA}) was quantified at a 40-ms delay from the peak of the dual eEPSC (27). Consistent with AMPAR-mediated eEPSCs that indicated increased PPF and reduced synapse number, we found reduced I_{NMDA} (genotype $P = 0.014$, two-way RM-ANOVA; Fig. 2*F*). Accordingly, the NMDA:AMPA ratio was not different ($P = 0.88$; Fig. 2*I*), suggesting that postsynaptic NMDAR numbers are unaffected by *Hip14* deletion. However, we did observe faster I_{NMDA} decay kinetics in *Hip14*$^{-/-}$ SPNs (Fig. 2*H*), raising the possibility of an alteration in NMDAR subunit composition.

Loss of Excitatory Synapses in *Hip14*$^{-/-}$ Hippocampal CA1 Neurons. Palmitoylation has been suggested as a regulator of synaptic plasticity (28, 29), and deficits in plasticity have been reported in HD models (17). To determine whether *Hip14* knockout alone influences synapse plasticity, we turned attention to the hippocampus, first characterizing basal synaptic transmission in CA1 pyramidal neurons. Whole-cell recordings of CA1 pyramidal neurons, unlike striatal SPNs, revealed no difference in membrane properties, action potentials, or firing rates (Fig. 3*A*), suggesting that such alterations are somewhat specific to SPNs in *Hip14*$^{-/-}$ mice. We saw no difference in mean or cumulative probabilities of sEPSC amplitudes ($P = 0.85$, two-way RM-ANOVA; Fig. 3*B*). However, like SPNs in *Hip14*$^{-/-}$ mice, there was a reduction in mean event frequency ($P < 0.0005$; Fig. 3*B*) and increases in IEI cumulative probabilities (genotype $P < 0.001$, two-way RM-ANOVA), suggesting that hippocampal synapse number is similarly reduced in these animals. Unlike SPNs, no difference in paired-pulse ratio (Fig. 3*C*) was observed, and AMPAR rectification was unaffected (Fig. 3*D*). Similarly to SPNs, the NMDA:AMPA current ratio (Fig. 3*E*) was unaffected. We also found no significant difference in either the decay kinetics (Fig. 3*F*) or ifenprodil sensitivity (Fig. 3*G*) of isolated NMDAR currents, suggesting that the synaptic content of GluN2B subunits is unaltered at CA1 synapses.

In agreement with our whole-cell results, we found no difference in the paired-pulse ratio of field potentials evoked in CA1 stratum radiatum (Fig. 4*A*). Field excitatory postsynaptic potential (fEPSP) fiber volley amplitudes were similar between genotypes across all stimulation intensities tested (Fig. 4*B*). However, we observed a diminished fEPSP slope in slices from *Hip14*$^{-/-}$ mice (interaction $P = 0.006$, two-way RM-ANOVA;

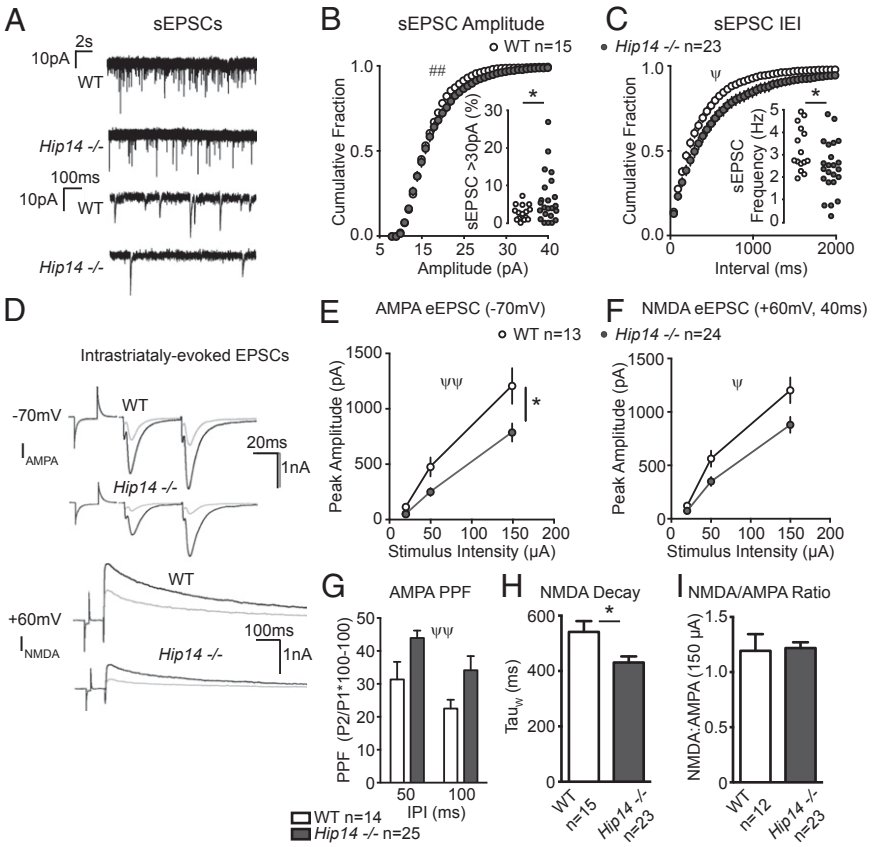

Fig. 2. Pre- and postsynaptic alterations to SPN glutamatergic synapses in *Hip14*$^{-/-}$ slices. (*A*) Voltage-clamp recordings of sEPSCs at V_h −70 mV in SPNs. (*B*) There was a significant interaction between genotype and event amplitude cumulative probabilities, due to more large events in *Hip14*$^{-/-}$ SPNs (*Inset*). (*C*) There was a significant genotype effect with increased sEPSC IEIs and reduced mean event frequency in *Hip14*$^{-/-}$ SPNs (*Inset*). (*D*) Stimulus evoked EPSCs (eEPSCs) carried by AMPARs (−70 mV, paired pulses, *Upper*) and NMDARs (+60 mV, single pulse, *Lower*) at 50 (gray) and 150 μA (black). *Hip14*$^{-/-}$ eEPSCs were significantly smaller for both AMPA-mediated (*E*) and NMDAR-mediated (*F*) currents. Paired-pulse facilitation of AMPAR currents was increased (*G*), whereas NMDAR eEPSC decay kinetics (weighted τ; *H*) were decreased in *Hip14*$^{-/-}$ SPNs. No differences in NMDA:AMPA ratio were observed (*I*). Repeated measures ANOVA ## interaction, P <0.01; ψ genotype, P < 0.05; ψψ genotype, P < 0.01. *t test, P < 0.05 (Bonferonni post-hoc in *E*). IPI, interpulse interval.

Fig. 4*C*), consistent with the reduced sEPSC frequency and again suggestive of a loss of functional excitatory synapses. Despite reductions in hippocampal volume (11), there were no significant differences in CA1 or CA3 cell counts between genotypes (P = 0.11, two-way ANOVA; Fig. 4*D*), suggesting volume reductions unrelated to pyramidal cell number. To confirm a loss of synapses in *Hip14*$^{-/-}$ CA1, we analyzed dendritic spine density by Golgi impregnation. In agreement with our conclusions from the electrophysiological data, we observed significantly reduced spine densities in CA1 pyramidal neurons of the stratum radiatum from *Hip14*$^{-/-}$ mice (P < 0.001, unpaired t test; Fig. 4*E*).

Impaired Hippocampal Long-Term Potentiation. Next, we investigated long-term potentiation at hippocampal CA3 Schaffer collateral to CA1 synapses. In WT animals, high-frequency stimulation (HFS; 100 Hz, 1 s × 3, 10-s intertrain interval) resulted in LTP whereas LTP was entirely absent in *Hip14*$^{-/-}$ mice (P = 0.02, unpaired t test of % potentiation 50–60 min post-HFS, herein; Fig. 4*F*), despite the clear posttetanic potentiation indicative of intact presynaptic short-term potentiation. To determine whether Hip14 is essential for LTP or whether the threshold for LTP induction is altered as a result of *Hip14* knockout, we facilitated the NMDAR dependence of this form of plasticity (30) by addition of the NMDAR coagonist glycine (10 + 2 μM strychnine). Under these conditions, LTP was partially restored to a level not significantly different from that in WT (P = 0.12; Fig. 4*G*). Finally, we combined this with a more robust induction protocol (3 × HFS separated by 5 min each)

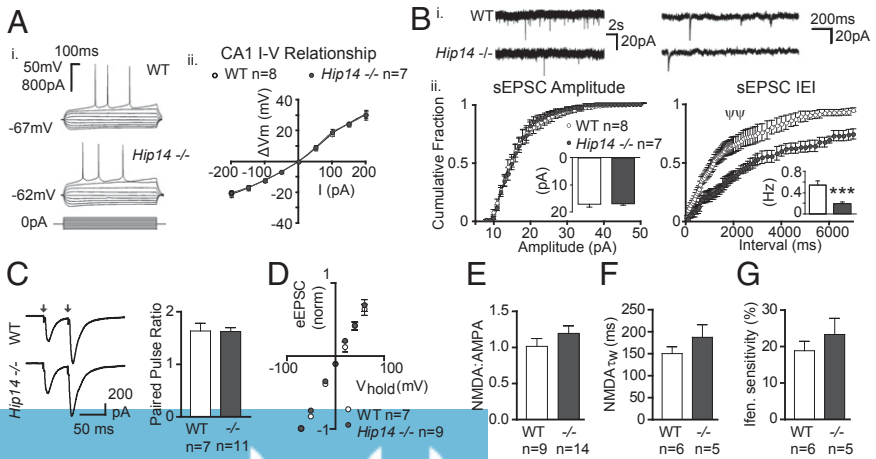

Fig. 3. Reduced sEPSC frequency in hippocampal CA1 pyramidal cells. (*A*) No differences were observed in CA1 current-clamp membrane potential responses (*i*, *Upper*) to 50-pA current injection steps (*i*, *Lower* and *ii*). (*B*) In CA1 voltage-clamp recordings of sEPSCs (−70 mV, i) there were no differences in event amplitudes (*ii*, *Left*), but there was a significant genotype effect on IEIs (*ii*, *Right*) and reduced mean event frequency in *Hip14*$^{-/-}$ (ii, *Right Inset*). (*C*) PPRs were similar, suggesting that decreased event frequency is due to reduced synapse number. (*D*) AMPAR-mediated rectification was unaltered. (*E*–*G*) NMDA:AMPA ratios (*E*), isolated NMDAR decay kinetics (*F*), and the ifenfprodil (ifen) sensitivity of isolated NMDAR currents (*G*) were also not significantly different. ψ,genotype. *t test; see text for details.

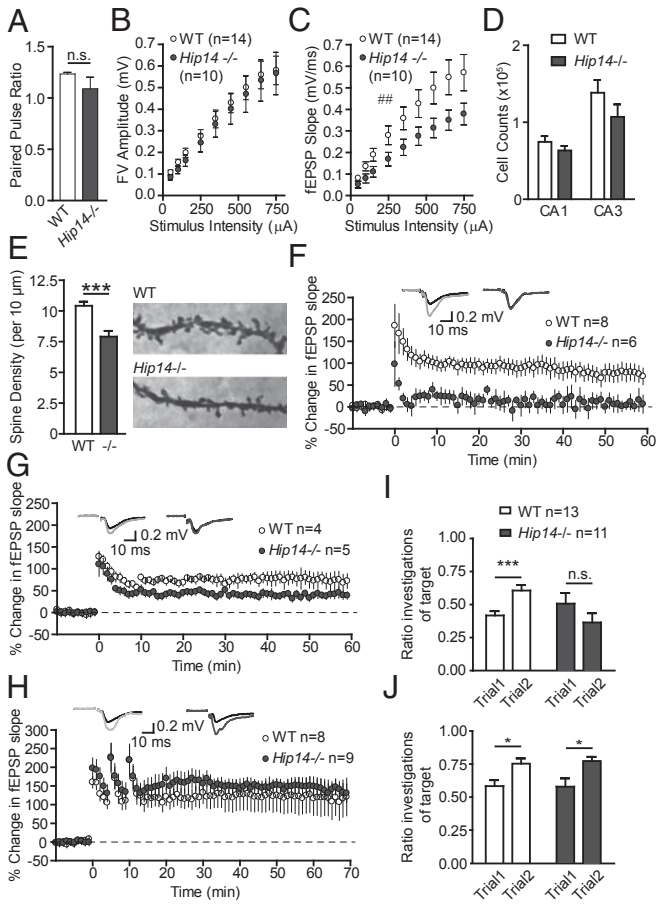

Fig. 4. Impaired LTP due to increased induction threshold and spatial memory deficits in *Hip14*$^{-/-}$ hippocampus. (*A* and *B*) fEPSP recordings in the stratum radiatum demonstrated no significant genotype difference in PPR (*A*) or fiber volley amplitudes (*B*). (*C*) fEPSP slope values were significantly reduced in *Hip14*$^{-/-}$ slices. (*D*) Total hippocampal cell counts showed no difference between WT and *Hip14*$^{-/-}$ mice. (*E*) Dendritic spine density was decreased in the stratum radiatum of Hip14$^{-/-}$ mice (cells: $n = 28$ for WT, 21 for *Hip14*$^{-/-}$). (*F*) Hippocampal slices from *Hip14*$^{-/-}$ mice displayed severe deficits in LTP using a stimulation protocol that induced reliable LTP in slices from WT mice. (*G*) The addition of glycine (10 μM) to the bath partially alleviated the *Hip14*$^{-/-}$ LTP deficit to levels not significantly different from WT. (*H*) Combining glycine (10 μM) with an enhanced stimulation protocol was sufficient to restore the LTP deficit to WT levels. (*I* and *J*) Learning a novel-object location (*I*) is impaired in *Hip14*$^{-/-}$ mice whereas the ability to recognize a novel object remains intact (*J*). For *F–H*, superimposed traces on the *Left* are from WT mice before (black) and 50–60 min after (light gray) high-frequency stimulation (HFS). Superimposed traces on the *Right* are from *Hip14*$^{-/-}$ mice before (black) and 50–60 min after (dark gray) HFS. #interaction, $P < 0.01$; **t* test, $P < 0.05$; ****t* test, $P < 0.001$.

and found that this completely restored LTP in *Hip14*$^{-/-}$ mice to WT levels ($P = 0.65$; Fig. 4*H*). Thus, the loss of a solitary palmitoyltransferase (*Hip14*$^{-/-}$) produces significant plasticity deficits, resulting in a markedly increased threshold for LTP induction. However, these deficits can be overcome by strong induction paradigms, demonstrating that the machinery required for LTP is intact, even if severely impaired.

Impaired Hippocampal-Dependent Memory. Serious hippocampal plasticity deficits should be reflected by impaired performance in hippocampal-dependent spatial learning tests such as novel-object location memory (31). As anticipated, WT animals spent more time investigating the relocated object in trial 2 ($P = 0.0002$, unpaired *t* test; Fig. 4*I*), demonstrating spatial memory reflected by clear preference for spatial novelty. In contrast, *Hip14*$^{-/-}$ mice failed to show any preference for the object in trial 2 ($P = 0.11$, unpaired *t* test; Fig. 4*I*), thus exhibiting a marked impairment in spatial memory. When tested in a perirhinal cortex-dependent novel object recognition task (31), in which one of a pair of familiar objects from trial 1 is replaced in trial 2 (same location), both WT ($P = 0.015$, paired *t* test) and *Hip14*$^{-/-}$ mice ($P = 0.004$, paired *t* test) spent significantly more time investigating the novel object (Fig. 4*J*). Thus, although object recognition memory is intact in *Hip14*$^{-/-}$ mice, they exhibit marked deficits in both hippocampal plasticity and spatial memory.

Discussion

Numerous PATs regulate palmitoylation in the mammalian brain. Despite considerable substrate overlap between these PATs, we found a number of electrophysiological and behavioral consequences induced by the loss of Hip14/DHHC17 alone. In the striatum we observed alterations in membrane properties and a reduction in spontaneous excitatory neurotransmission, likely due to both reduced synapse numbers (11) and decreased Pr. Perhaps most striking, however, was the profound impairment of hippocampal LTP and spatial memory in *Hip14*$^{-/-}$ mice. Our data confirm a clear role for palmitoylation in synaptic function and suggest that HIP14 dysfunction in HD may account for a number of synaptic and plastic deficits. Furthermore, our results highlight a major modulatory requirement of Hip14 in the gating of hippocampal synaptic plasticity and the formation of spatial memory.

We previously reported a decrease in excitatory synapses in the striatum of *Hip14*$^{-/-}$ mice (11), suggesting deficits in excitatory transmission to the basal ganglia. Consistently, we found here that SPNs from *Hip14*$^{-/-}$ mice had reduced spontaneous excitatory event frequencies and evoked current amplitude. We, and others, have shown that spine formation and maintenance in SPNs is dependent upon an intact glutamatergic network (32, 33); it is tempting to suggest that synapse reductions in *Hip14*$^{-/-}$ mice result from a breakdown in structural connectivity, driven by impaired transmission. A critical role for Hip14 in transmitter release has been described in *Drosophila* (14), and our conclusions are further supported by the identification of SNAP-25 and synaptotagmin as HIP14 substrates (12, 14). However, no Pr alterations were observed in CA1 neurons, suggesting that release deficits are not global.

Hip14 deletion was sufficient to impair hippocampal LTP and performance on a spatial memory task. We found that fEPSP responses were diminished in *Hip14*$^{-/-}$ stratum radiatum, which, together with the observed decrease in sEPSC frequency and reduction in spine density, is highly suggestive of fewer excitatory synapses. It is unlikely that this alone can account for the LTP deficit, as we saw no correlation between the initial response size and the amount of potentiation 50–60 min post-HFS ($r^2 = 0.11$, $P = 0.42$). Furthermore, the conditions that restored LTP to WT levels (glycine and enhanced stimulation) would be expected to influence existing synapses rather than recruit additional synapses.

The idea that protein palmitoylation can influence synaptic plasticity has been previously suggested (2). As the growing list of palmitoylated neural proteins includes a variety of surface receptors, scaffolding proteins, and vesicle fusion proteins among others, the precise mechanism by which *Hip14* knockout impairs LTP is difficult to pinpoint and remains to be determined. NMDAR subunits are palmitoylated at two cysteine clusters; palmitoylation of cluster 1 enhances synaptic stability whereas palmitoylation of cluster 2 increases retention within the Golgi and reduces surface expression (9). In the present study, NMDA:AMPA ratios were unaffected in both the striatum and hippocampus, suggesting a lack of up- or down-regulation of synaptic NMDARs following *Hip14* knockout and arguing against significant depalmitoylation at cluster 1 (34). Moreover,

we also rule out the possibility that the observed LTP deficit is due to a change in the composition of synaptic NMDARs as NMDAR decay kinetics and ifenprodil sensitivity were unaffected in *Hip14* knockouts.

AMPAR subunits, which are HIP14 substrates (13), are palmitoylated at two different cysteines; palmitoylation of the TMD-2 cysteine promotes accumulation in the Golgi and prevents forward trafficking to the surface, whereas depalmitoylation of the C-terminal cysteine enhances PKC phosphorylation of nearby serines, association with 4.1N, and insertion into the membrane (7, 35). We did observe a significant increase in a subset of large AMPAR-mediated EPSCs in *Hip14*$^{-/-}$ SPNs, which may be a consequence of depalmitoylation-induced release from the Golgi. Interestingly, although depalmitoylation of the C-terminal cysteine enhances extrasynaptic insertion events of AMPA receptors, these receptors are not stable as the authors found no evidence of increases in steady-state AMPAR surface expression (7). This suggests that some degree of AMPAR palmitoylation is required for surface retention. Such stability within the membrane would be absolutely essential for LTP, which is significantly impaired at *Hip14*$^{-/-}$ CA1 synapses.

It has also been shown that palmitoylation of scaffolding proteins PSD-95 (28) and A-kinase anchoring protein 79/150 (29) is required for LTP in cultured hippocampal neurons, and recent work has highlighted the importance of certain SNARE family vesicle fusion proteins in LTP expression (36), some of which are recognized or candidate palmitoylated proteins (37). Thus, our observed LTP deficit may result from depalmitoylation of a number of synaptic proteins. We have previously reported reduced PSD-95 and SNAP-25 palmitoylation in brain tissue from *Hip14*$^{-/-}$ mice (11). Although our results do not provide a definitive conclusion regarding the mechanism of impaired LTP, our findings are clearly behaviorally relevant as highlighted by impairments in hippocampal-dependent memory. That said, perirhinal cortex-dependent novel-object recognition (31) was not altered, suggesting that *Hip14* knockout does not result in global memory deficits and that certain neuronal networks are more vulnerable than others.

In vitro expression studies have revealed considerable overlap between PAT substrates. For example, multiple PATs in addition to HIP14, including DHHC2, -3, -5, and -7, are able to palmitoylate PSD-95 (2, 38). Due to this apparent lack of substrate specificity, one might expect a similar overlap of the cellular and behavioral phenotypes of various DHHC-deficient animal lines. However, the PAT–substrate relationship in vivo will depend on the expression levels and localization of both the substrates and the PATs themselves within individual cells. Perhaps it is not surprising, then, that considerable phenotypic differences exist among the DHHC-deficient mice. DHHC8 knockout mice have sexually dimorphic alterations in locomotor activity and prepulse inhibition (39), whereas DHHC-5–deficient mice exhibit impaired fear conditioning and are born at half the expected rate (40). Furthermore, polymorphisms in the human DHHC8 gene are implicated in schizophrenia (39), whereas human DHHC9 and 15 mutations are associated with X-linked mental retardation (41, 42). Thus, despite partial in vitro substrate overlap, relatively specific substrate effects occur in single PAT knockouts. Moreover, in the present study, we found deficits in striatal neurons that were not present in CA1 cells, demonstrating that the loss of a single PAT does not affect all networks equally.

Although wild-type huntingtin interacts with HIP14 and enhances its PAT activity, this interaction is reduced in the presence of mutant huntingtin (16). *Hip14*$^{-/-}$ mice recapitulate some of the behavioral, biochemical, and neuropathological deficits observed in HD, and Hip14 function is reduced in HD mice (11). Interestingly, nearly all of the striatal cellular and synaptic changes observed here are reminiscent of those in various HD models, albeit at late stages of phenotype progression (17, 18). In the present study, we were able to observe electrophysiological changes within the striatum of 3- to 6-wk-old *Hip14*$^{-/-}$ mice that do not occur in HD models until months later. Also, SPN loss and striatal volume reductions are evident at birth in *Hip14*$^{-/-}$ mice (11), whereas the striatal degeneration in HD, and in HD mice, progresses over time (17).

It is interesting to note that several HD mouse models demonstrate impaired, but not absolute, loss of LTP at the earliest stages of their phenotype progression (19, 21–23, 43). In addition to our findings here, those findings in HD mice suggest that palmitoylation deficits may underlie early synaptic dysfunction in HD mice, which may contribute to early cognitive deficits reported in prodromal HD carriers (44, 45). Thus, manipulations aimed at enhancing protein palmitoylation may be a valuable strategy to combat early cognitive symptoms in HD.

Materials and Methods

Animals were housed and maintained according to the Canadian Council on Animal Care and all procedures were approved by the University of British Columbia Committee on Animal Care. Experiments were conducted on the same *Hip14*$^{-/-}$ mouse line that was previously characterized (11). All data are expressed as mean ± SEM, and the statistical analyses used included Student *t* test and two-way ANOVA as detailed in the text.

Electrophysiology. Standard whole-cell patch-clamp striatal recordings were obtained from 400-μm coronal slices from ~30-d-old male mice as previously described (24), with recording conditions adapted from ref. 46 to contain 10 mM glucose and as detailed in the text. Horizontal hippocampal slices (400 μm) were prepared as previously described (47), and plasticity experiments were produced as in ref. 30 and as described in the text. Both whole-cell and field responses were evoked by 40-μs stimulation pulses delivered through a glass micropipette placed within 200–400 μm of the recording site.

Cell Counts. Mice were terminally anesthetized by i.p. injection of 2.5% (vol/vol) avertin and perfused with 3% (vol/vol) paraformaldehyde/0.15% glutaraldehyde in PBS. Mouse brains were fixed in the same solution for 24 h at 4 °C followed by cryoprotection in 30% (vol/vol) sucrose. Brains were frozen on dry ice and cut into coronal sections (25 μm) using a cryostat microtome (HM 500 M, Microm International). Every eighth section throughout the hippocampus spanning from Bregma −0.94 to −2.8 mm was stained with an antibody reactive to NeuN (Chemicon), a marker of neuronal nuclei, as described previously (48). CA1 and CA3 hippocampal subregions were delineated in every eighth NeuN-stained section using a 2.5× objective, and then cells were counted using a 40× objective on a Zeiss Axio Imager M2 microscope with a motorized computer-controlled stage (Ludl Electronics) and a CX9000 Digital CCD video camera (Microbrightfield). Total estimated number of CA1 and CA3 neurons was obtained using the Fractionator Probe in StereoInvestigator 9, a morphometry and stereology software package (MicroBrightField) with a 25- × 25-μm counting frame and 150- × 150-μm grid size. Overall, the coefficient of error was <0.1. All quantification was conducted with the investigator blind to genotype.

Spine Analysis. Animals were transcardially perfused with PBS and Golgi impregnated using the FD Rapid GolgiStain kit (FD Neurotechnologies) following the manufacturer's instructions. Final steps were performed on 150-μm-thick coronal sections (cut by cryostat at −22 °C) before coverslip and permount application.

Dendrites were imaged with an oil-immersion lens at 63× magnification using a Zeiss Axiovert 200M microscope. Analysis was restricted to the posterior stratum radiatum, and dendrite collaterals off the apical dendrite of CA1 pyramidal neurons were chosen as regions of interest (ROI). Images were collected throughout the depth of the tissue at 2-μm steps in the z-plane and converted to TIFF files, and spines were counted manually in ImageJ with the experimenter blinded to genotype. Long dendritic protrusions lacking a clear head were excluded from the analysis. Two to three ROIs were averaged for each cell, and seven cells were analyzed per animal (animal $n = 4$ for WT; $n = 3$ for *Hip14*$^{-/-}$).

Novel-Object Location and Recognition Testing. Novel-object testing took place in open 50- × 50-cm black plastic boxes with 16-cm sides. Testing occurred over a period of 2 d, and the same cohort of animals was used for both the novel-object location task (conducted on day 1) and the novel-object

recognition task (conducted on day 2). Recordings were collected using the automated behavioral analysis software Ethovision (Noldus) via live video collected from a ceiling-mounted video camera. On day 1, mice were exposed to the box for 10 min before being removed for 5 min. Two different novel objects were then placed in the upper corners of the box, far enough from the edges to allow movement around the perimeter. Mice were then reintroduced to the box in the lower left corner, and their movements were recorded for 5 min. The number of investigations of both the novel objects was scored (trial 1). Mice were then removed from the box, and the object in the top right corner was moved to the lower right corner. Mice were reintroduced to the box again for another 5 min, and then the number of investigations of the objects was scored (trial 2). On day 2, the 10-min exposure and trial 1 were identical to that on day 1. However, in trial 2 of day 2, the object in the top right corner was replaced with a different and unfamiliar object positioned in the top right corner. The number of investigations was recorded for a 5-min period.

ACKNOWLEDGMENTS. The authors thank Nagat Bissada, Mahsa Amirabassi, and Shaun Sanders for their animal care services. This work was supported by grants from the Canadian Institutes of Health Research (MOP-81144 and Emerging Team Grant GPG-102165) and the Cure Huntington's Disease Initiative. A.J.M. received fellowships from the Canadian Institutes of Health Research, Huntington's Society of Canada, and the Huntington's Disease Society of America. M.P.P. is a recipient of a Michael Smith Foundation for Health Research Postdoctoral Fellowship. F.B.Y. is supported by the Canadian Institutes of Health Research-Institute of Genetics Walter and Jessie Boyd and Charles Scriver MD/PhD studentship. M.R.H. is a Killam University Professor and holds a Canada Research Chair in Human Genetics and Molecular Medicine.

1. el-Husseini Ael-D, Bredt DS (2002) Protein palmitoylation: A regulator of neuronal development and function. *Nat Rev Neurosci* 3(10):791–802.
2. Fukata Y, Fukata M (2010) Protein palmitoylation in neuronal development and synaptic plasticity. *Nat Rev Neurosci* 11(3):161–175.
3. El-Husseini Ael-D, et al. (2002) Synaptic strength regulated by palmitate cycling on PSD-95. *Cell* 108(6):849–863.
4. Ho GP, et al. (2011) S-nitrosylation and S-palmitoylation reciprocally regulate synaptic targeting of PSD-95. *Neuron* 71(1):131–141.
5. Craven SE, El-Husseini AE, Bredt DS (1999) Synaptic targeting of the postsynaptic density protein PSD-95 mediated by lipid and protein motifs. *Neuron* 22(3):497–509.
6. Yang G, Xiong W, Kojic L, Cynader MS (2009) Subunit-selective palmitoylation regulates the intracellular trafficking of AMPA receptor. *Eur J Neurosci* 30(1):35–46.
7. Lin DT, et al. (2009) Regulation of AMPA receptor extrasynaptic insertion by 4.1N, phosphorylation and palmitoylation. *Nat Neurosci* 12(7):879–887.
8. Gladding CM, Raymond LA (2011) Mechanisms underlying NMDA receptor synaptic/extrasynaptic distribution and function. *Mol Cell Neurosci* 48(4):308–320.
9. Hayashi T, Thomas GM, Huganir RL (2009) Dual palmitoylation of NR2 subunits regulates NMDA receptor trafficking. *Neuron* 64(2):213–226.
10. Young FB, Butland SL, Sanders SS, Sutton LM, Hayden MR (2012) Putting proteins in their place: Palmitoylation in Huntington disease and other neuropsychiatric diseases. *Prog Neurobiol* 97(2):220–238.
11. Singaraja RR, et al. (2011) Altered palmitoylation and neuropathological deficits in mice lacking HIP14. *Hum Mol Genet* 20(20):3899–3909.
12. Huang K, et al. (2004) Huntingtin-interacting protein HIP14 is a palmitoyl transferase involved in palmitoylation and trafficking of multiple neuronal proteins. *Neuron* 44(6):977–986.
13. Huang K, et al. (2009) Neuronal palmitoyl acyl transferases exhibit distinct substrate specificity. *FASEB J* 23(8):2605–2615.
14. Ohyama T, et al. (2007) Huntingtin-interacting protein 14, a palmitoyl transferase required for exocytosis and targeting of CSP to synaptic vesicles. *J Cell Biol* 179(7):1481–1496.
15. Yanai A, et al. (2006) Palmitoylation of huntingtin by HIP14 is essential for its trafficking and function. *Nat Neurosci* 9(6):824–831.
16. Huang K, et al. (2011) Wild-type HTT modulates the enzymatic activity of the neuronal palmitoyl transferase HIP14. *Hum Mol Genet* 20(17):3356–3365.
17. Milnerwood AJ, Raymond LA (2010) Early synaptic pathophysiology in neurodegeneration: Insights from Huntington's disease. *Trends Neurosci* 33(11):513–523.
18. Raymond LA, et al. (2011) Pathophysiology of Huntington's disease: Time-dependent alterations in synaptic and receptor function. *Neuroscience* 198(198):252–273.
19. Murphy KP, et al. (2000) Abnormal synaptic plasticity and impaired spatial cognition in mice transgenic for exon 1 of the human Huntington's disease mutation. *J Neurosci* 20(13):5115–5123.
20. Smith R, Brundin P, Li JY (2005) Synaptic dysfunction in Huntington's disease: A new perspective. *Cell Mol Life Sci* 62(17):1901–1912.
21. Milnerwood AJ, et al. (2006) Early development of aberrant synaptic plasticity in a mouse model of Huntington's disease. *Hum Mol Genet* 15(10):1690–1703.
22. Usdin MT, Shelbourne PF, Myers RM, Madison DV (1999) Impaired synaptic plasticity in mice carrying the Huntington's disease mutation. *Hum Mol Genet* 8(5):839–846.
23. Lynch G, et al. (2007) Brain-derived neurotrophic factor restores synaptic plasticity in a knock-in mouse model of Huntington's disease. *J Neurosci* 27(16):4424–4434.
24. Milnerwood AJ, Raymond LA (2007) Corticostriatal synaptic function in mouse models of Huntington's disease: Early effects of huntingtin repeat length and protein load. *J Physiol* 585(Pt 3):817–831.
25. Nisenbaum ES, Wilson CJ (1995) Potassium currents responsible for inward and outward rectification in rat neostriatal spiny projection neurons. *J Neurosci* 15(6):4449–4463.
26. Bindman LJ, Meyer T, Prince CA (1988) Comparison of the electrical properties of neocortical neurones in slices in vitro and in the anaesthetized rat. *Exp Brain Res* 69(3):489–496.
27. Thomas MJ, Beurrier C, Bonci A, Malenka RC (2001) Long-term depression in the nucleus accumbens: A neural correlate of behavioral sensitization to cocaine. *Nat Neurosci* 4(12):1217–1223.
28. Ehrlich I, Malinow R (2004) Postsynaptic density 95 controls AMPA receptor incorporation during long-term potentiation and experience-driven synaptic plasticity. *J Neurosci* 24(4):916–927.
29. Keith DJ, et al. (2012) Palmitoylation of A-kinase anchoring protein 79/150 regulates dendritic endosomal targeting and synaptic plasticity mechanisms. *J Neurosci* 32(21):7119–7136.
30. Milner AJ, Cummings DM, Spencer JP, Murphy KP (2004) Bi-directional plasticity and age-dependent long-term depression at mouse CA3-CA1 hippocampal synapses. *Neurosci Lett* 367(1):1–5.
31. Barker GR, Warburton EC (2011) When is the hippocampus involved in recognition memory? *J Neurosci* 31(29):10721–10731.
32. Kaufman AM, et al. (2012) Opposing roles of synaptic and extrasynaptic NMDA receptor signaling in cocultured striatal and cortical neurons. *J Neurosci* 32(12):3992–4003.
33. Segal M, Greenberger V, Korkotian E (2003) Formation of dendritic spines in cultured striatal neurons depends on excitatory afferent activity. *Eur J Neurosci* 17(12):2573–2585.
34. Mattison HA, Hayashi T, Barria A (2012) Palmitoylation at two cysteine clusters on the C-terminus of GluN2A and GluN2B differentially control synaptic targeting of NMDA receptors. *PLoS ONE* 7(11):e49089.
35. Hayashi T, Rumbaugh G, Huganir RL (2005) Differential regulation of AMPA receptor subunit trafficking by palmitoylation of two distinct sites. *Neuron* 47(5):709–723.
36. Jurado S, et al. (2013) LTP requires a unique postsynaptic SNARE fusion machinery. *Neuron* 77(3):542–558.
37. Kang R, et al. (2008) Neural palmitoyl-proteomics reveals dynamic synaptic palmitoylation. *Nature* 456(7224):904–909.
38. Greaves J, Chamberlain LH (2011) DHHC palmitoyl transferases: Substrate interactions and (patho)physiology. *Trends Biochem Sci* 36(5):245–253.
39. Mukai J, et al. (2004) Evidence that the gene encoding ZDHHC8 contributes to the risk of schizophrenia. *Nat Genet* 36(7):725–731.
40. Li Y, et al. (2010) DHHC5 interacts with PDZ domain 3 of post-synaptic density-95 (PSD-95) protein and plays a role in learning and memory. *J Biol Chem* 285(17):13022–13031.
41. Raymond FL, et al. (2007) Mutations in ZDHHC9, which encodes a palmitoyltransferase of NRAS and HRAS, cause X-linked mental retardation associated with a Marfanoid habitus. *Am J Hum Genet* 80(5):982–987.
42. Mansouri MR, et al. (2005) Loss of ZDHHC15 expression in a woman with a balanced translocation t(X;15)(q13.3;cen) and severe mental retardation. *Eur J Hum Genet* 13(8):970–977.
43. Simmons DA, et al. (2009) Up-regulating BDNF with an ampakine rescues synaptic plasticity and memory in Huntington's disease knockin mice. *Proc Natl Acad Sci USA* 106(12):4906–4911.
44. Orth M, et al. (2010) Abnormal motor cortex plasticity in premanifest and very early manifest Huntington disease. *J Neurol Neurosurg Psychiatry* 81(3):267–270.
45. Stout JC, et al. (2011) Neurocognitive signs in prodromal Huntington disease. *Neuropsychology* 25(1):1–14.
46. Milnerwood AJ, et al. (2010) Early increase in extrasynaptic NMDA receptor signaling and expression contributes to phenotype onset in Huntington's disease mice. *Neuron* 65(2):178–190.
47. Petkau TL, et al. (2012) Synaptic dysfunction in progranulin-deficient mice. *Neurobiol Dis* 45(2):711–722.
48. Slow EJ, et al. (2003) Selective striatal neuronal loss in a YAC128 mouse model of Huntington disease. *Hum Mol Genet* 12(13):1555–1567.